Geophysical Research Letters

Supporting Information for

A new divergence method to quantify methane emissions using observations of Sentinel-5P TROPOMI

Mengyao Liu[1]*, Ronald Van der A[1,2], Michiel Van Weele[1], Henk Eskes[1], Xiao Lu[3], Pepijn Veefkind[1,4], Jos de Laat[1], Hao Kong[5], Jingxu Wang[6], Jiyunting Sun[1], Jieying Ding[1], Yuanhong Zhao[6], Hongjian Weng[5]

[1] KNMI, Royal Netherlands Meteorological Institute, De Bilt, the Netherlands

[2] Nanjing University of Information Science & Technology (NUIST), Nanjing, China

[3] School of Engineering and Applied Sciences, Harvard University, Cambridge, MA 02138, USA

[4] Delft University of Technology, Delft, The Netherlands

[5] Department of Atmospheric and Oceanic Sciences, School of Physics, Peking University, Beijing, China

[6] College of Oceanic and Atmospheric Sciences, Ocean University of China, Qingdao, China

* Correspondence to: Mengyao Liu (mengyao.liu@knmi.nl)

This PDF file includes 15 pages containing

1. Part A: The stripe correction on XCH_4
2. Part B: Influence of surface albedo corrections on estimated CH_4 emissions
3. Figures S1 to S8
4. Table S1
5. SI references

Part A. The stripe correction on XCH_4

We apply the stripe correction on XCH_4 to remove across-track biases between the individual viewing angles of the satellite. The stripe correction is determined from Level 2 files by first applying a high-pass median filter in the across-track direction and next a high-pass median filter in the time direction (Borsdorff, personal communication 2020). The Level 2 files provide the data in two dimensions as scan lines (temporal direction) and ground pixels (across satellite track and approximately west-east). The first step for creating the stripe correction is performed per orbit. First a smoothed XCH_4 image is computed using a median filter in the across track direction, using the XCH_4 with qa_value > 0.5 for each ground pixel and its four eastern and western neighbors. At the eastern and western edge of the swath this number is less, but at least 4 neighboring pixels are taken into account. In this step, online scans with at least 20% valid data are taken into account. The across track striping pattern of the orbit is computed by subtracting the smoothed image from the XCH_4 data and subsequently taking the median in the temporal direction.

After computing the stripe pattern for all orbits, a smoothing between the orbits is performed by applying a median of the orbit and its 50 previous and 50 next orbits (note that 100 orbits cover approximately one week of data). Finally, a linear interpolation is performed in temporal direction to compute the striping correction for all orbits, including those for which too little data was available to compute the stripe pattern.

As shown in Figure S1, the corrections depend on the TROPOMI ground pixel index and orbit number. The changes of yearly averaged XCH_4 in 2019 before and after destriping

are within ±5 ppb (mean: −0.08 ppb) on a 0.25° grid. Figure S1 shows the difference with time before and after the stripe correction. For most ground pixels, the differences are within 10 ppb.

Part B. Influence of surface albedo corrections on estimated emissions

The current official TROPOMI bias-corrected XCH_4 product (XCH_4^{S5P}) is derived from a second order fit to the ratio of TROPOMI and GOSAT CH_4 as a function of SWIR albedo [*Hasekamp et al.*, 2019; *Lorente et al.*, 2021]. It is defined as:

$$XCH_4^{S5P} = XCH_4\,(c1 + c2 \cdot A + c3 \cdot A2) \qquad (S1)$$

where A is the surface albedo retrieved at the SWIR spectral range and c1 (=1.0173), c2 (=−0.1538), c3 (=−0.2036) are the correction parameters derived from a second order fit of the ratio of TROPOMI and GOSAT CH_4 as a function of albedo [*Hasekamp et al.*, 2019]. Although this posteriori correction reduces the general biases to ground-based TCCON observation, XCH_4^{S5P} is still likely to underestimate over the areas with low albedos and overestimate over very bright surface. These systematic biases can be seen clearly over Northern Africa in Fig S2, which covers a wide range of realistic surface albedos. The positive corrections given by Eq. (S1) for the areas with high albedos (>0.5) lead to high XCH_4^{S5P} comparing to uncorrected XCH_4 (Fig S2 (c)). Thus， the spatial pattern of XCH_4^{S5P} (Fig. S2 (b)) are quite similar to the SWIR surface albedo (Fig. S2 (d)). These biases of XCH_4^{S5P}, caused by the dependence on GOSAT observations and the lack of ground-based observations, have been also found by *Lorente et al.* [2021]. The new fitting function for the coming version becomes independent of GOSAT observations and monotonous (See Figure 4 in *Lorente et al.* [2021]).

To avoid the abovementioned biases caused by surface albedos, in this study, a piecewise linear fit to XCH_4 as a function of the corresponding SWIR surface albedo are designed to give a positive correction for low-albedo areas (< 0.1) and a negative correction for high-albedo areas (≥ 0.1). The junction point, where the albedo is equal to 0.1, of the piecewise linear fit functions is obtained from *Hasekamp et al.* [2019]. The advantage of the linear fitting is that the coefficient can be directly treated as correction factor (CF).

Therefore, the corrected TROPOMI XCH_4 (XCH_4^{CORR}) is $XCH_4 \cdot (1 + CF)$. CF is obtained as follows:

$$CF = CF_1 \cdot (0.1 - A) \quad (A < 0.1) \quad (S2)$$

$$CF = CF_2 \cdot A \quad (A \geq 0.1) \quad (S3)$$

where CF_1 is the positive-correction coefficient (= 671.0), and CF_2 is the negative-correction coefficient (= −63.5) derived from the two-segment linear fitting.

The fitting is based on the gridded yearly average of TROPOMI XCH_4 and corresponding SWIR surface albedo in 2019 over the US (the domain is showed in Fig. 2) on a 0.25° grid (the same spatial resolution as the later divergence calculation and the emission estimation). Only XCH_4 retrievals lower than 3000 ppb and with an elevation below 500 m are selected for the fitting. We use gridded data instead of observation pixels to avoid issues with seasonal variations and over-sampling.

Figure S3(a)-(b) are the spatial distributions of TROPOMI yearly-averaged XCH_4 after destriping and SWIR surface albedo corrections over the North America on a 0.25° grid in 2019. Some strong enhancements caused by landforms (e.g., rocks and deserts in Utah and Arizona; alluvial accumulation around Mississippi Delta) are clearly seen from Fig. 3(a). Figure 3(d) gives a more reasonable spatial pattern over North America. The overestimated XCH_4 due to the bare ground in western U.S. decrease while the concentration over the east coast increase after corrections (Fig. S3(d)). After converting XCH_4 to XCH_4^{PBL}, the spatial distribution of CH_4 becomes more continuous over mountains in Fig. S3(e). Despite the uncertainty from surface albedo corrections, enhancement of CH_4 are found over Texas, California and Appalachia regions when comparing to the regional background (Fig. S3(f)).

The third row presents spatial distributions of XCH_4 with the surface albedo corrections of the official S5P operational product (XCH_4^{S5P}). The overestimated XCH_4 due to the bare ground (i.e. high albedo) in western U.S. decrease after both corrections (Fig. S3 (d) and (g)). Relatively big differences in the two corrections are found over the east coast of the U.S., where our results are about ~15 ppb higher than XCH_4^{S5P} over the areas with dark surfaces (albedo < 0.1). The enhancements caused by wetlands over here are much

clearer in our corrections. The underestimation of XCH_4^{S5P} has also been improved in Lorente et al, [2021].

Figure S3 further quantified the difference caused by two different surface albedo corrections over Texas. In general, the locations of big sources are caught in both Fig. S4 (a) and (b). Big differences of estimated emissions appear over Mexico and the east of Texas. The big sources near the border of Lousiana and Texas in Fig. S4(b) seem to be biases in XCH_4^{S5P}.

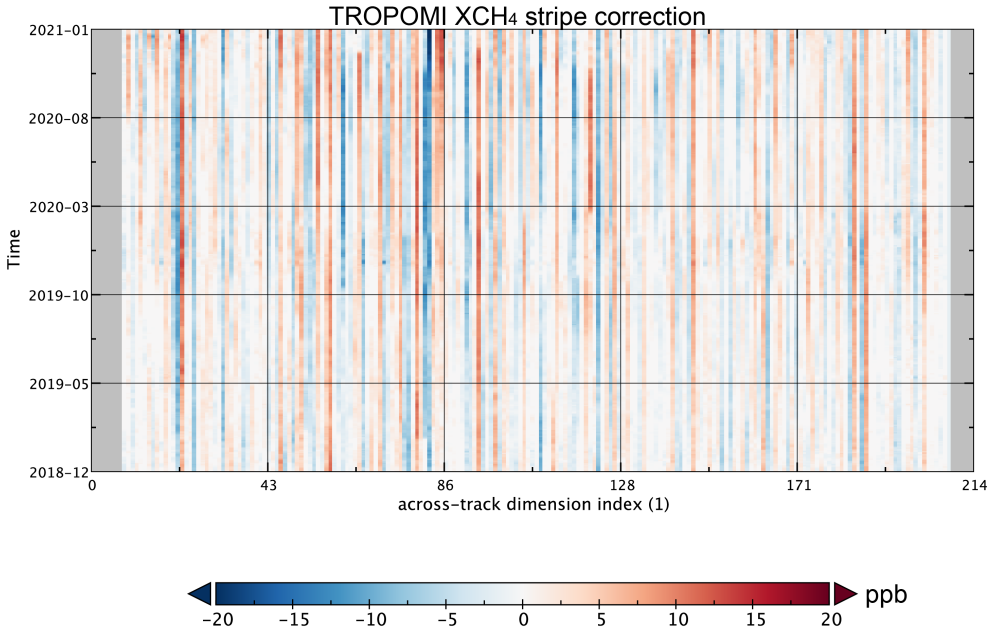

116

117 **Figure S1.** The difference over time before and after the stripe correction.

118

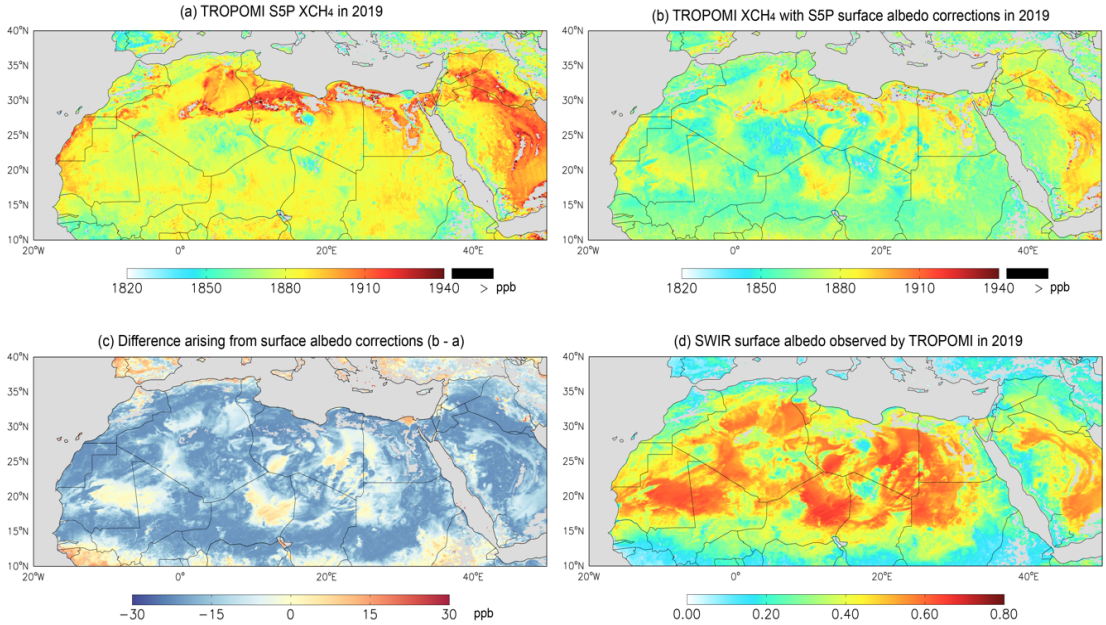

119 **Figure S2.** The spatial distributions of yearly averaged (a) XCH_4, (b) XCH_4^{S5P} and (c)
120 their difference in 2019 on a 0.25° grid. (d) The TROPOMI observed SWIR surface
121 albedos that is used to correct XCH_4.

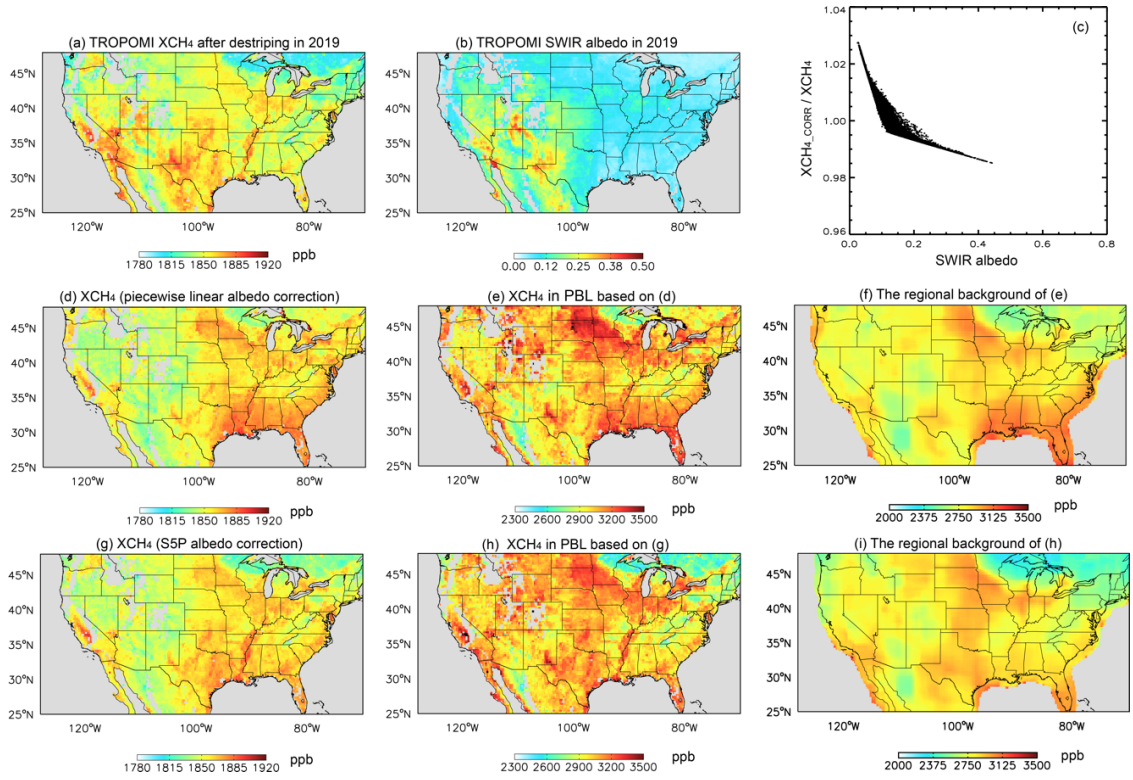

Figure S3. Yearly averages of (a) TROPOMI XCH_4 after destriping and (b) TROPOMI SWIR surface albedo in 2019 on a 0.25° grid. (c) The scatter plots of the ratios of XCH_{4_CORR}/XCH_4 and SWIR surface albedos. Each dot represents a grid cell in (a) and (b). Yearly averages of (d) XCH_4 with segment linear surface albedo corrections, (e) the corresponding XCH_4 in PBL and (f) its regional background. (g)-(i) are similar to (d)-(f) but for XCH_4 with S5P surface albedo correction.

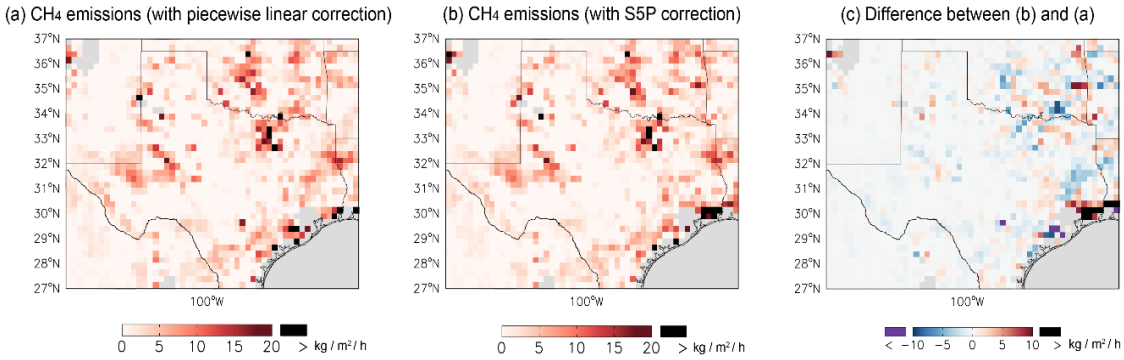

Figure S4. The estimated CH_4 emissions based on (a) XCH_4^{CORR}, (b) XCH_4^{S5P} and (c) their difference in 2019 on a 0.25° grid.

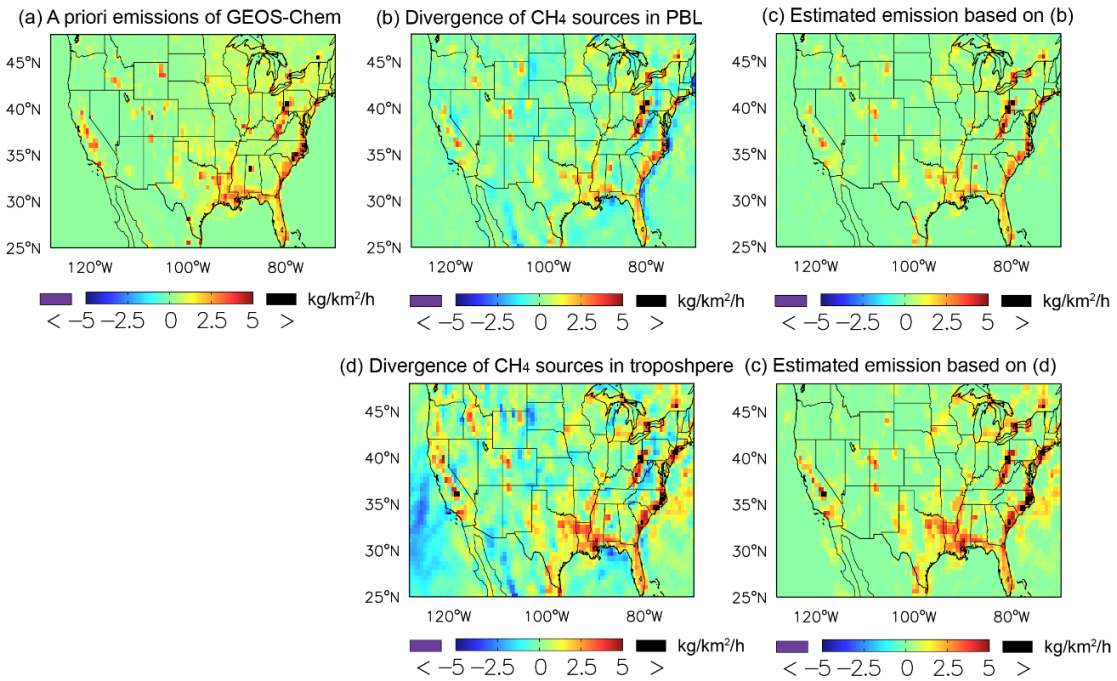

Figure S5. The spatial distributions of (a) the average of a priori CH_4 emissions used in GEOS-Chem simulation, (b) the divergence of CH_4 sources in the PBL, and (c) corresponding estimated CH_4 emissions over July-September 2012 on a 0.625° lon. × 0.5° lat. grid. (d)-(e) are similar to (b)-(c) but for the results using XCH_4 in the troposphere.

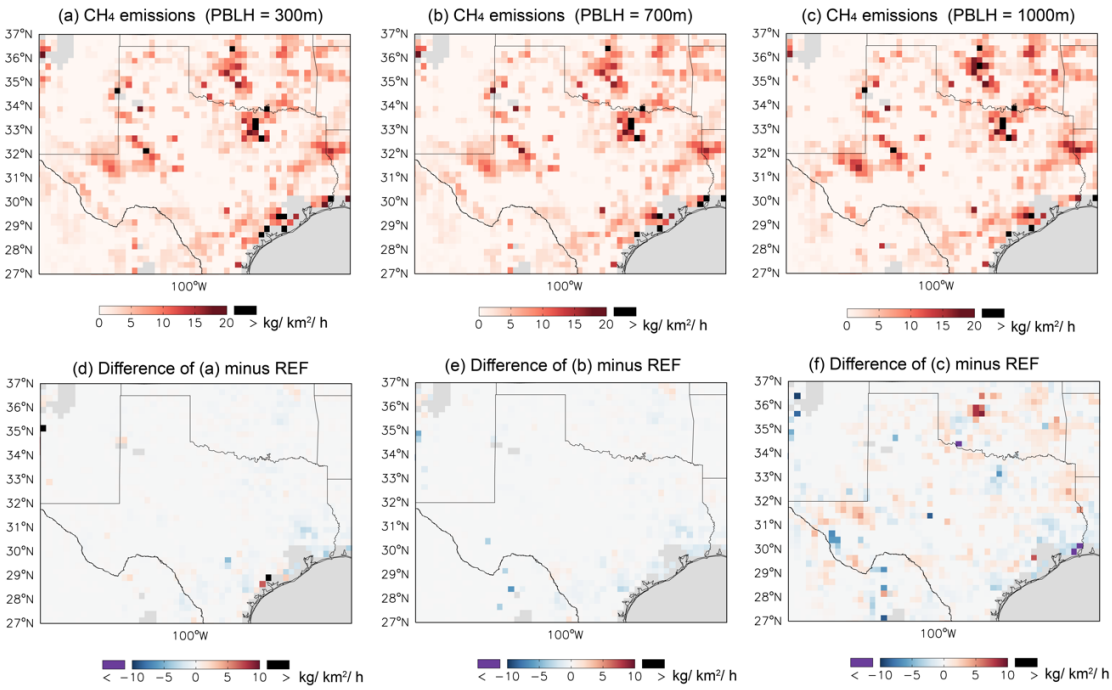

Figure S6. Results of different assumptions on PBLH. (a)-(c) are CH_4 emissions estimated with (a) PBLH = 300 m, (b) PBLH = 700 m, (c) PBLH = 1000 m and. (d)-(f) are corresponding differences of (a)-(c) minus REF.

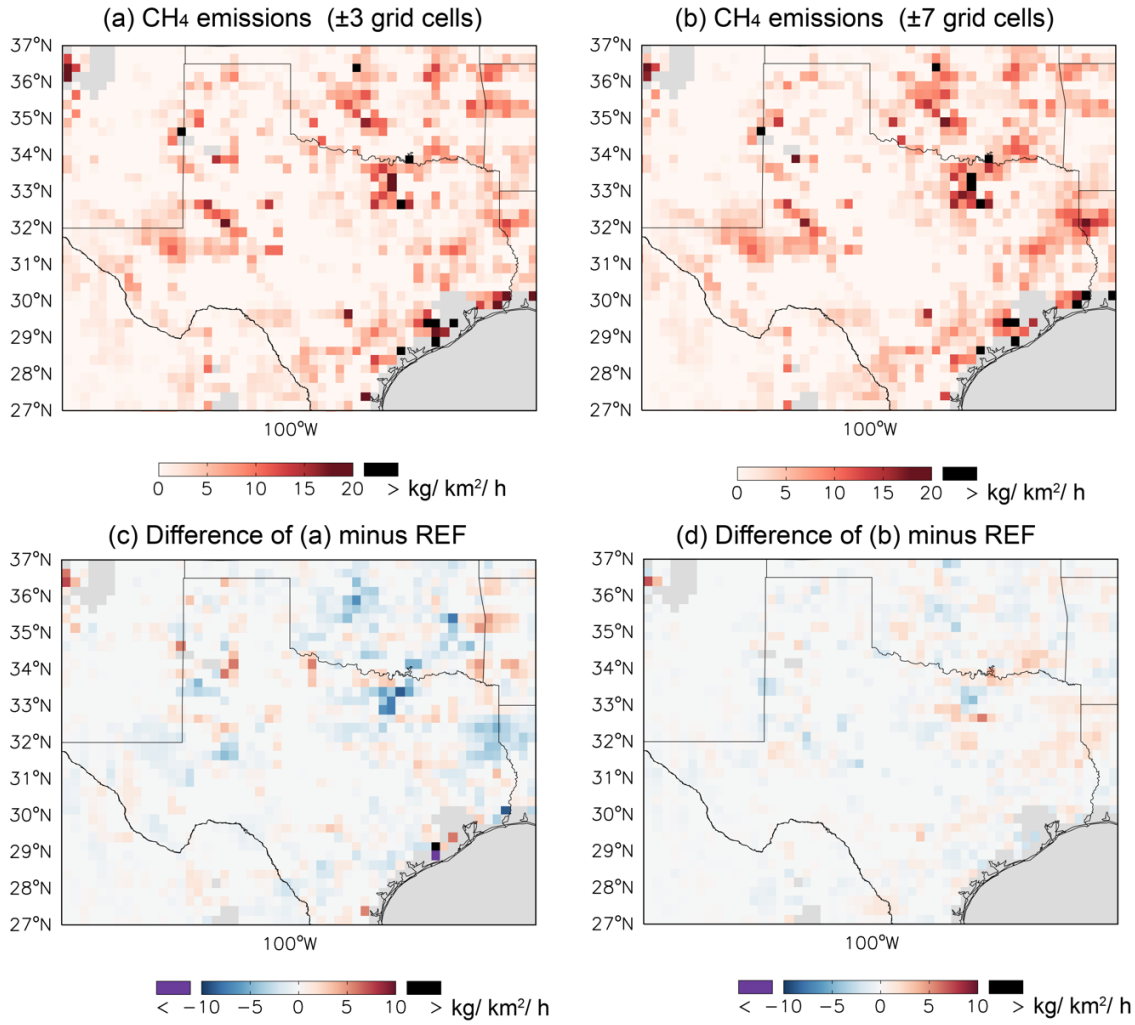

142 **Figure S7.** Results of different assumptions on the size of the background region from (a)
143 surrounding 3 grid cells to (b) 7 grid cells (in each direction). (c)-(d) are corresponding
144 differences of (a)-(b) minus REF.

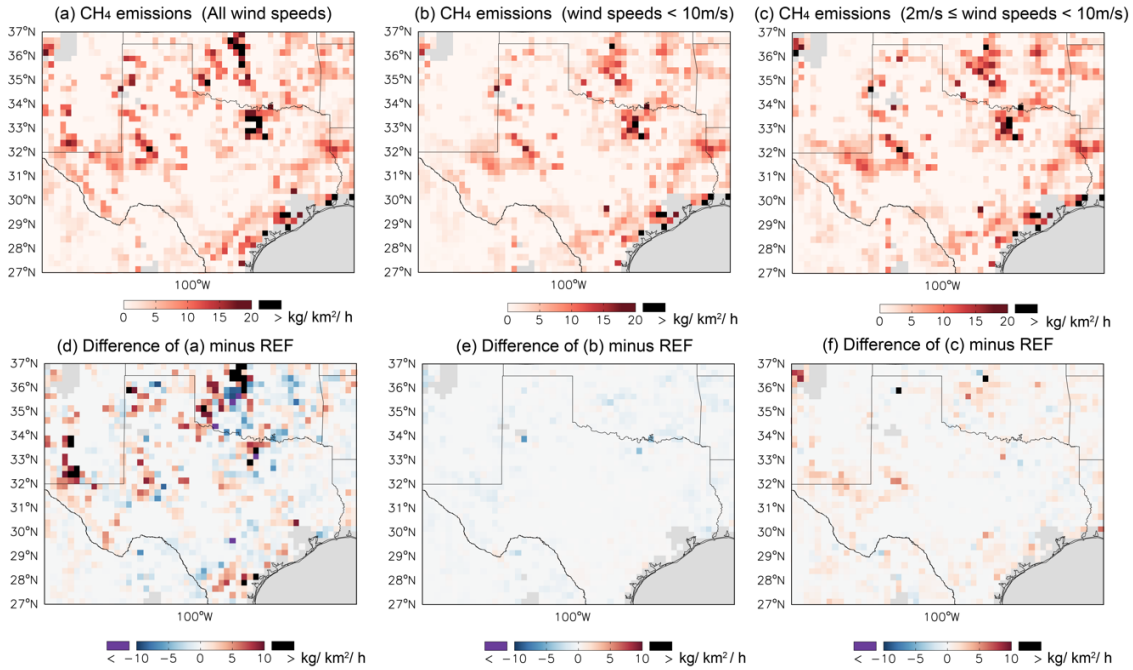

Figure S8. Results of different assumptions on the constraints of wind speeds (V). (a)-(c) are CH_4 emissions estimated with (a) all V, (b) V < 10 m/s, (c) 2 m/s < V < 10 m/s. (d)-(f) are corresponding differences of (a)-(c) minus REF.

Table S1. Results of sensitivity studies.

REF: 1 < V < 10 m/s; PBLH = 500m; Background: ±5 grid cells; 3.06 Tg a^{-1}

Difference with reference to REF[1]	Mean ($kg/km^2/h$)	Medium ($kg/km^2/h$)	Min ($kg/km^2/h$)	Max ($kg/km^2/h$)	Total emission of Permian Basin[4] ($Tg\ a^{-1}$)
Wind speeds (m/s)					
V < 10	−0.2	−0.1	−10.4	1.44	2.82
2 < V < 10	0.5	0.3	−4.7	14.7	3.78
All	0.1	0.0	−29.8	30.5	3.60
PBLH (m)[2]					
300	−0.05	0.0	−4.5	6.8	3.06
700	−0.1	−0.02	−6.2	1.9	3.04
1000	0.07	0.1	−22.4	9.2	3.37
Background[3]					
±3 grid cells	−0.3	−0.2	−12.0	11.2	2.87
±7 grid cells	0.0	0.0	−4.4	7.1	3.00

[1] The value of mean, medium, minimum and maximum is the difference with the reference (REF) in the domain (27°-37°N, 106.5°-93°W) of Fig. 4.

[2] The PBLH is the height above the ground.

[3] The tested parameter is the number of surrounding grid cells that are used to generate the background.

[4] The domain of the Permian Basin is 30°-34°N, 101°-105°W, shown in Fig. 4(a)

References:

Hasekamp, O., A. Lorente, H. Hu, A. Butz, J. aan de Brugh, and J. Landgraf (2019), Algorithm Theoretical Baseline Document for Sentinel-5 Precursor Methane Retrieval(1.10).

Lorente, A., et al. (2021), Methane retrieved from TROPOMI: improvement of the data product and validation of the first 2 years of measurements, *Atmos. Meas. Tech.*, *14*(1), 665-684.